Bad Metals Made with Good-Metal Components

S. B. Arnason, S. P. Herschfield, and A. F. Hebard
Department of Physics, University of Florida, Gainesville, Florida 32611
(Received 22 December 1997; revised manuscript received 12 June 1998)

We have grown thin stable films of a good metal, Ag, that have characteristics of bad metals: high resistivity, strong temperature dependence of resistivity, and lack of resistive saturation. For films of different thickness, the temperature-dependent resistance and the Hall effect resistance provide evidence that the apparent bad metallicity is a consequence of the microstructure of the film rather than the result of new physics. This microstructure, which we characterize with scanning probe techniques, occurs on length scales comparable to the mean free path, thereby changing the sign of the classical magnetoresistance from positive to negative. [S0031-9007(98)07453-5]

PACS numbers: 73.50.Jt

Many of the most exciting new materials discovered in the past two decades can be classified as "bad metals." Distinguishing characteristics of metals in this category include an anomalously high resistivity scale and the absence of resistivity saturation at high temperature [1]. These characteristics imply an electronic mean free path, l, which is shorter than the physically reasonable length scales in the problem and are seen in materials such as alkali-doped C_{60} [2], high-T_c superconductors [3], and the itinerant ferromagnet $SrRuO_3$ [4]. When l is shorter than the interatomic spacing or the inverse Fermi wave vector, k_F^{-1}, the Boltzmann theory of transport is not self-consistent [5]. This boundary of self-consistency has been drawn with several criteria (i.e., the Ioffe-Regel limit $k_F l > 1$ or the Mooij limit $\rho < 100\text{–}150\ \mu\Omega\,\mathrm{cm}$) [6,7], and good metals deviate from a metallic temperature dependence of resistivity at or near these demarcations [8,9].

We have studied thin films of a good metal, silver (Ag), which can be made to mimic bad metals. Prepared with the proper microstructure, these films have extremely high effective resistivities and anomalously large temperature dependences of their resistivities, but their Hall effect remains that of bulk Ag. The residual resistivity and temperature dependence of resistivity are linearly related—a single multiplicative scale factor maps the resistivity data for a given film onto that of a thick silver film. Most intriguingly, these films have a negative magnetoresistance which is quadratic in the applied field. This magnetoresistance has the same magnitude as the classical magnetoresistance, $\Delta R/R \sim -(\omega_c \tau)^2$, where ω_c is the cyclotron frequency and τ is the scattering time, but with the opposite sign. Using microscopic imaging techniques, scanning electron microscopy (SEM), atomic force microscopy (AFM), and electrostatic force microscopy (EFM), we are able to characterize the microstructure that leads to these transport anomalies. The anomalous magnetoresistance is determined to be a consequence of microstructure having characteristic length scales comparable to the electron mean free path.

The films discussed in this paper were grown by thermal evaporation of Ag onto glass substrates at room temperature in a vacuum lower than 10^{-7} Torr and at a rate of 1 Å per minute. The thickness, d, was determined by monitoring the amount of deposited mass with a quartz crystal monitor calibrated with the thickness measured by AFM. By measuring resistance *in situ*, during deposition, we were able to identify films by their location in the sequence of the stages of growth (Fig. 1). Initially, the growth proceeds by nucleation of isolated Ag clusters. These clusters grow by surface diffusion of the arriving adatoms. Eventually, the cluster sizes become large enough to coalesce and form discrete, continuous paths. Finally, the film becomes homogeneous, a medium of well-connected microscopic grains. The films discussed below are too thin to show classical size effects in the resistivity, a regime where the electronic transport in Ag is well understood [10], but

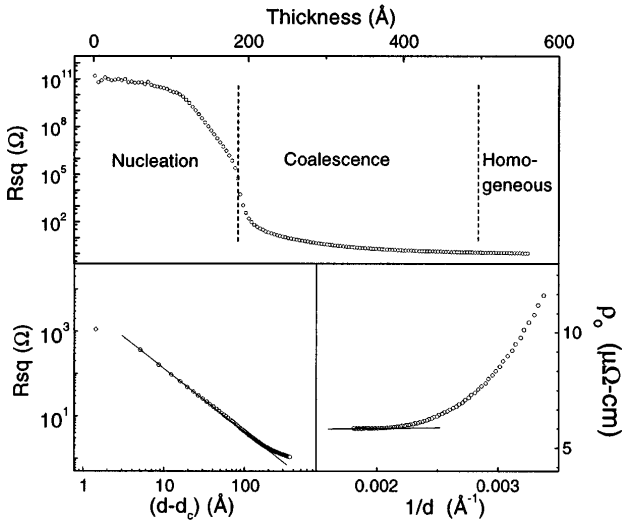

FIG. 1. Resistance as a function of coverage for a 560-Å-thick film (top panel). Below 100 Å, nucleation of isolated grains. From 100 to 200 Å, growth of isolated islands. From 200 to 400 Å, coalescence of islands. From 400 to 500 Å, crossover to classical size effect. From 500 Å on, classical size effects. The bottom right panel shows classical size effect scaling of resistivity, $\rho \to \rho_0$ for $1/d \to 0$. The bottom left panel shows power law scaling of resistance with deviation from critical thickness, $R \sim (d - d_c)^{-\eta}$, $\eta = 1.3 \pm 0.1$, and $d_c = 192$ Å.

 0031-9007/98/81(18)/3936(4)$15.00

thicker than quench-condensed films used to study weak localization [11].

Both the coalescence and homogeneous regions can be quantitatively identified. The lower right-hand panel of Fig. 1 shows the resistivity as a function of inverse thickness, d^{-1}. For thickness greater than 450 Å, resistivity is linear in d^{-1}, in agreement with classical size-effect theories of [12,13]. Extrapolation of the solid line to the origin ($d \to \infty$) gives $\rho_0 = 5.9\ \mu\Omega$ cm, a reasonable value for films grown under these conditions. The lower left-hand panel of Fig. 1 shows a linear dependence of the log of resistance on the log of $(d - d_c)$, where d_c is a critical thickness. In the thickness range $d_c < d < 400$ Å the resistance is a power law in thickness, $(d - d_c)^{-\eta}$. This scaling of resistance as a power law in a thickness difference has been previously observed in thin gold films and interpreted in terms of percolation theory [14]. The bad-metal films in this paper have thicknesses varying between 280 and 330 Å and are all from this coalescence regime, relatively far from the percolation threshold, d_c. The actual resistance of a film in this regime is very sensitive to the details of growth: substrate preparation, rate of growth, base pressure, etc. These variables affect the critical coverage at which coalescence occurs. However, by monitoring the resistance during the growth process, we can controllably arrest the growth process to produce stable films with reproducible transport properties that can be further characterized *ex situ*.

The temperature-dependent resistivity is shown in Fig. 2 for a series of Ag films grown in the coalescence regime. Both the residual resistivity ρ_0 and the temperature dependence as measured by an approximately linear resistivity slope $d\rho/dT$ are significantly enhanced relative to bulk behavior, represented by the 560-Å-thick film with growth characteristics shown in Fig. 1 and which is also the bottom-most curve in Fig. 2. As can be seen in the inset of Fig. 2, ρ_0 is directly proportional to $d\rho/dT$. This proportionality suggests that there is a common source for the renormalization that gives rise to anomalously high resistivity scales. The discrepancy arises because resistivity is calculated by multiplying the measured sheet resistance R by the measured film thickness d. With this procedure we are using a thickness and aspect ratio which seriously overestimates the effective thickness of the film and underestimates the contribution of the longer paths that the currents must follow. The resistivity is therefore enhanced by the microscopic geometry of the film, not by any change in the physics of conduction. The simple act of rescaling the resistivity calculation by the correct geometrical factor will cause all of the curves in Fig. 2 to collapse onto a single curve representing transport in bulk material. This interpretation is consistent with our finding that the Hall coefficients of our samples are unchanged. This simple phenomenon, proportional enhancement of ρ_0 and $d\rho/dT$, is a signature of tortuous conduction paths and extremely thin links enhancing the calculated resistivity. That films in the coalescence regime would require

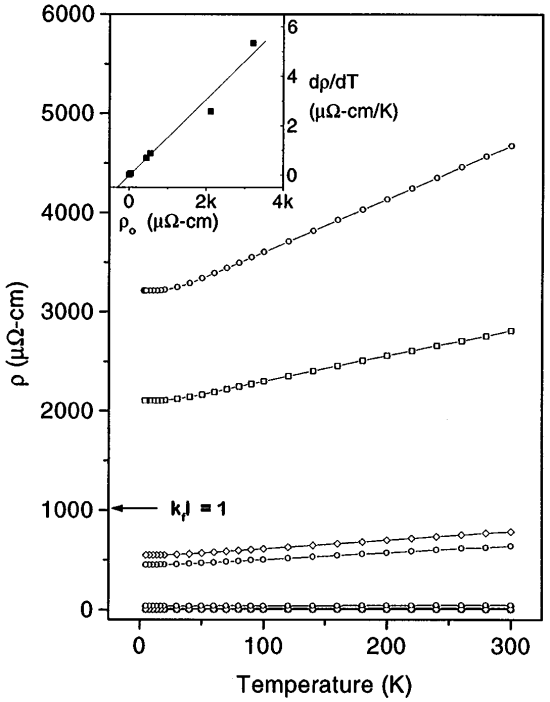

FIG. 2. Resistivity as a function of temperature for a series of Ag films grown at room temperature. The film with the lowest resistivity is the 560 Å thick film whose growth is shown in Fig. 1. Its $d\rho/dT$ is that of bulk silver. As the films become thinner and approach the critical thickness for coalescence, both ρ_0 and $d\rho/dT$ increase with a common scale factor. The inset shows the linear relation of $d\rho/dT$ with ρ_0.

some geometric renormalization to account for the sample inhomogeneity is not surprising, but that this term could be of order 1000 in a 300-Å-thick film is surprising. The conduction paths must be very thin, narrow, and twisting, *but at the same time they are composed of material having the conductivity of bulk Ag metal*. A less dramatic geometric enhancement may be occurring in the alkali-metal-doped fullerenes, where Refs. [2,15] indicate that ρ_0 and $d\rho/dT$ of Rb_3C_{60} are roughly a factor of 2 higher than ρ_0 and $d\rho/dT$ of K_3C_{60}. Clearer examples of this geometric effect are seen in sintered bulk samples of $YBa_2Cu_3O_x$ [16] and thin epitaxial films of $Ba_{1-x}K_xBiO_3$ [17]. In the YBCO case the microstructure of a sintered pellet is analogous to partially connected Ag grains. In epitaxial BKBO films there are strains that are induced by changes in oxygen stoichiometry which may introduce cracking and, as a result, complicated current paths.

Characterization of the surface topography with scanning electron microscopy and atomic force microscopy has provided insights into the nature of microstructure that is responsible for the strong geometric renormalization of the resistivity. The AFM micrographs show films composed of grains with an average diameter of 500 Å which appear to be densely packed on the surface of the substrate. Careful examination of the topography on length scales comparable to the grain size shows that, while some gaps between grains extend to the substrate, the vast majority

do not, suggesting a film that is already well connected. In contrast to the AFM images, SEM micrographs, taken with the incident electron beam normal to the surface of the film, show the topography of a globular, percolative cluster with a clear separation between the conducting silver and the nonconducting intergrain material. Both microscopy techniques have problems measuring the thin and narrow gaps between grains; AFM is limited by the small but finite size of the scanning probe tip, and SEM is insensitive to thin layers on an insulating substrate. Neither technique measures the electrical coupling between grains. To understand this coupling, we have employed electrostatic force microscopy [18,19].

Electrostatic force microscopy images the local surface potential, weighted by the effective, local capacitance between the cantilever and the sample [18]. With the sample grounded, the EFM micrograph (taken simultaneously with AFM data) shows features that are related to the topography of the sample via the changing capacitance. With a bias applied to the sample, the EFM signal changes. The features, which still contain topographical information, separate into two domains, one at low potential, the other at high. While we have not yet been able to completely separate the two signals and thereby resolve the conducting and nonconducting portions of our films, the structure of the domains is fairly clear. The high potential portion of the film is filamentary with domains that tend to have a width of 1 to 3 grains. The lower potential portion of the film is composed of larger structures with an average width of 3 to 5 grains. Although we cannot *a priori* determine which is the globally connected conducting portion of the film, it is clear that both domains are tenuous and interpenetrating on submicron length scales.

The most dramatic impact of the microstructure on transport is seen in the negative magnetoresistance (Fig. 3), measured with the field normal to the sample surface. Our understanding of these data is based on the recognition that transport is dominated by electron flow in narrow tortuous channels having a typical width, w, on the order of the bulk transport scattering length, $l_0 \sim 300$ Å. In this configuration much of the resistance is due to diffusive scattering at the channel boundaries. Two regimes can be identified and are discussed below: a low-field weak-localization regime at low temperatures, and a higher-field classical regime at high temperatures.

The low temperature magnetoresistance peak (Fig. 3) can be fitted with the standard functional form for weak localization in 2D [11], but the parameters extracted from the fits are not consistent with the scattering rates implied by the resistivity measurements. Attempts to include theoretically predicted [20] flux cancellation that occurs when there is boundary scattering in constrained channels qualitatively account for the higher field scales but do not yield consistent scattering times. Experimental work on quasi-one-dimensional wires in GaAs-based heterostructures [21,22] has demonstrated these flux cancellation corrections, but these systems, in contrast to our Ag films,

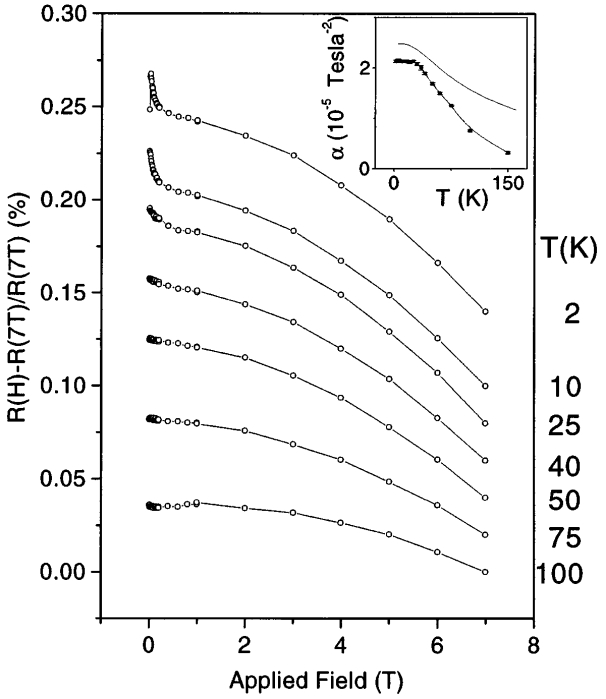

FIG. 3. Change in resistance with applied magnetic field at various temperatures, normalized to the resistance at 7 T with the curves offset for clarity. The low-field peak, seen at low temperatures, is due to weak localization. The high-field behavior is quadratic. The inset shows the temperature dependence of the coefficient extracted by fitting the high-field data to a parabola, line with markers, and $(\omega_c\tau)^2/H^2 = [R_H/\rho(T)]^2$, line.

have straight channels with well-defined boundaries. It is possible that extensions of theory to include surface asperities and tortuous paths could model the weak-localization behavior of our system.

The high-field magnetoresistance is negative and quadratic in the applied field, in contrast to the *positive* magnetoresistance seen in bulk Ag and observed in our thickest film (Fig. 1 and bottom-most trace of Fig. 2). Fitting the high-field data to a parabola, we extract a coefficient α $[R(H) - R(0)/R(0) \sim -\alpha H^2]$. The magnitude and temperature dependence α (Fig. 3 inset) is consistent with the classically expected magnetoresistance, $\alpha = (\omega_c\tau)^2/H^2$, which we estimate from our Hall effect and resistivity measurements of a thick Ag film $(\omega_c\tau)^2 = [HR_H/\rho(T)]^2$ (solid line in Fig. 3 inset). This shows good qualitative agreement without the use of any fitting parameters, but does not explain the sign change.

The sign change can be understood with a simple classical model, a narrow twisting channel or wire with diffuse boundary scattering. In a straight wire, where the channel width is less than a mean free path, the majority of the conductivity comes from electrons that travel down the center of the channel. A small applied magnetic field increases resistance because it deflects electrons traveling down the center into the sides of the wire. In high fields, $R_c < 0.55w$, where w is the channel width,

straight channels show a negative resistance. In this case, the electrons are in cyclonic orbits and for a straight wire can again travel down the center of the wire, unaffected by the boundaries. This gives rise to reduced backscattering and negative magnetoresistance. These effects have been seen in systems with straight channels [23]. In our Ag films, $R_c \sim 7$ μm at 7 T, a value significantly larger than the width inferred from both the transport measurements (Fig. 2) and the scanning probe characterizations. Our samples are therefore in the low-field regime where the boundary scattering models for straight channels predict positive magnetoresistance. With a curved wire, the situation differs; all straight paths hit the edges. A circular orbit in a magnetic field can actually allow the electrons to travel farther without hitting the sides of the wire, producing a negative magnetoresistance. Thus, the origin of this effect is that a small magnetic field helps an electron around a curve, but would always hinder its travel down a straight wire.

To test this hypothesis, we have performed a simple calculation, based on prior theoretical treatments [24,25] of electronic transport in narrow, straight channels with diffusive boundary scattering. We consider a two-dimensional annular channel with inner radius r and width w. The boundary scattering is diffusive and no bulk scattering is considered. We ignore bulk scattering because the inferred mean free path at which the magnetoresistance saturates (Fig. 3 inset) is comparable to the channel widths observed in EFM, implying that we are in the clean limit. The resistivity is computed using the semiclassical Boltzmann equation with the approach described by Pippard [25]. In the limit of the radius of the annulus being much larger than the width, $r \gg w$, the magnetoresistance of the annulus reduces to that of a straight wire. However, when r is comparable or only a few times larger than w, the magnetoresistance of the annulus differs from that of a wire. In particular, at low applied fields the magnetoresistance is of the form $\Delta R/R = (\omega_c \tau)^2 F(r/w)$, where the function F is negative and of order unity for values of r/w that are consistent with the microstructure of our films, $1 < r/w < 10$. Our simple model thus predicts a negative magnetoresistance with a magnitude consistent with that observed in our films.

In summary, we have described the growth and characterization of thin Ag films which possess an anomalous negative magnetoresistance together with apparent resistivities that seem to violate the assumptions necessary for the application of Boltzmann transport theory. We have identified the microstructural origin of the geometric renormalization that explains the scale of the resistivity and can identify a signature for it, namely, the proportionality of the enhancement of ρ_0 and $d\rho/dT$. Finally, we establish the connection between the heretofore unrecognized negative classical magnetoresistance and the underlying tortuous microstructure of the films. The observed new phenomenology depends more on how the system is assembled than on what composes it.

We appreciate the contributions of Fred Sharifi and Heather Hudspeth in providing and interpreting SEM images, and we are grateful for the useful insights arising from discussions with Dimitri Maslov and Harold Baranger. We are also grateful to Phil Allen for pointing out that BKBO might exhibit similar "bad-metal" behavior. All scanning probe microscopy was done with a Park Scientific Autoprobe CP. This work was supported by the NSF, Contracts No. DMR-9705224 and No. DMR-9357474, and the National High Magnetic Field Laboratory.

[1] V. J. Emery and S. A. Kivelson, Phys. Rev. Lett. **74**, 3253–3256 (1995).
[2] A. F. Hebard, T. T. M. Palstra, R. C. Haddon, *et al.*, Phys. Rev. B, Rapid Commun. **43**, 9945–9948 (1993).
[3] M. Gurvitch and A. T. Fiory, in *Novel Superconductivity. Proceedings of the International Workshop on Novel Mechanisms of Superconductivity*, edited by S. A. Wolf and V. Z. Krezin (Plenum, Berkeley, CA, 1987), pp. 663–677.
[4] L. Klein *et al.*, Phys. Rev. Lett. **77**, 2774–2777 (1996).
[5] P. B. Allen *et al.*, Phys. Rev. B **34**, 4331–4333 (1986).
[6] C. C. Tsuei, Phys. Rev. Lett. **57**, 1943–1946 (1986).
[7] J. H. Mooij, Phys. Status Solidi A **17**, 521 (1973).
[8] D. W. Woodard and G. D. Cody, Phys. Rev. **136**, A166 (1964).
[9] V. A. Marchenko, Sov. Phys. Solid State **15**, 1261 (1973).
[10] P. B. Allen, Phys. Rev. B **36**, 2920–2923 (1987).
[11] G. Bergmann, Z. Phys. B **48**, 5–15 (1982).
[12] K. Fuchs, Proc. Camb. Philos. Soc. **34**, 100 (1938).
[13] E. H. Sondheimer, Adv. Phys. **1**, 1–42 (1952).
[14] A. Palevski *et al.*, J. Phys. Lett. **45**, L-367 (1984).
[15] X.-D. Xiang *et al.*, Nature (London) **361**, 54–56 (1993).
[16] J. Halbritter *et al.*, Z. Phys. B **71**, 411–413 (1988).
[17] E. S. Hellman and J. E. H. Hartford, Phys. Rev. B **47**, 11 346–11 353 (1993).
[18] Y. Martin, C. C. Williams, and H. K. Wickramasinghe, Appl. Phys. Lett. **52**, 1103 (1987).
[19] J. E. Stern *et al.*, Appl. Phys. Lett. **53**, 2717 (1988).
[20] C. W. J. Beenakker and H. v. Houten, Phys. Rev. B **38**, 3232–3240 (1988).
[21] Ç. Kurdak *et al.*, Phys. Rev. B **46**, 6846–6856 (1992).
[22] H. Z. Zheng *et al.*, Phys. Rev. B **34**, 5635–5638 (1986).
[23] K. Forsvoll and I. Holwech, Philos. Mag. **9**, 435 (1964).
[24] C. W. J. Beenakker and H. v. Houten, *Quantum Transport in Semiconductor Nanostructures* (Academic Press, New York, 1991).
[25] A. B. Pippard, *Magnetoresistance in Metals* (Cambridge University Press, Cambridge, England, 1989).